Desalination and Water Treatment
www.deswater.com
doi: 10.5004/dwt.2020.25335

184 (2020) 267–281
April

Selective adsorption of lanthanum ions with recyclable materials and experimental design using response surface methodology

Zhiguo Xiao, Yue Cheng*, Hongwei Yu, Jianyu Li

School of Material Science and Engineering, Jingdezhen Ceramic Institute, Jingdezhen 333403, China,
emails: cy_jci@163.com (Y. Cheng), zhiguox_jci@qq.com (Z. Xiao), 187162323@qq.com (H. Yu), 904674864@qq.com (J. Li)

Received 28 March 2019; Accepted 10 December 2019

ABSTRACT

It is necessary to better separate and recover rare earth elements from acid solution. The adsorbent that magnetic tripod ligand was synthesized was used to selectively adsorb lanthanum (La (III)). The adsorbent was characterized by transmission electron microscope, X-ray diffraction and Fourier-transform infrared spectroscopy. The adsorption effect of the adsorbent was studied by single-factor experiments, wherein the single factors included dosage, time, interfering ions and pH. For better predicting the test results, we used response surface methodology (RSM) to analyze the interaction between every single factor. Also, experiments on adsorbent recovery were carried out, and the adsorption mechanism was briefly discussed. The results of the study indicated that the magnetic tripod ligand was successfully synthesized. The predicted removal rate of La(III) can reach 99.42% by RSM with the dosage of 0.8 g/L, time of 100 min, and pH of 5. Moreover, the experimental results showed that the removal rate of lanthanum ion could reach 97.9%. After five cycles of reuse of the adsorbent, the adsorption effect was reduced to 78%. The reason for the high removal of La(III) by the adsorbent may be the important role of coordination chelation.

Keywords: Adsorption; Rare earth elements; Magnetic; Response surface methodology

1. Introduction

With the development of modern science and technology, the number of waste electrical and electronic equipment (WEEE) [1] is also increasing. This leads to how to recycle WEEE has become an urgent problem. Unlike conventional wastes, such wastes often contain a small number of heavy metals, precious metals, high value-added metals and so on [2], such as rare earth elements [3]. Rare earth elements are no longer only used in traditional fields, such as metallurgical industry, petrochemical industry, glass ceramics, etc. They are also used in LED flat panel displays [4], high-temperature superconductors, smart phones [5] and so on. Their unique physical and chemical properties make them very important and irreplaceable in the field of high and new technology [6]. However, rare earth elements are a kind of non-renewable resources; if they cannot be recovered from secondary resources, then it will be a huge waste of resources.

The main methods of disposal of WEEE are chemical treatment [7], pyrometallurgy [8], mechanical treatment [9], electrochemical method [10], etc. Compared with other methods, chemical treatment has the characteristics of higher efficiency, milder operation conditions and higher purification rate [11]. Generally speaking, only when the electronic waste is converted from solid to liquid phase can it be more conducive to the recovery of rare earth, so that chemical treatment may be the best choice. The chemical treatment method is to put crushed electronic waste particles into acidic or alkaline liquids. The leachate in the chemical treatment method is then extracted, precipitated, displaced, ion-exchanged, filtered and distilled to obtain high-grade metals [12]. Among them, leaching rare earth with an acid solution is the most common method.

* Corresponding author.

For example, recovering rare earth from nickel-hydrogen batteries requires acid leaching of rare earth [13].

In order to recover rare earth from acidic leaching solution, the adsorption method should be considered most. Adsorption method has the characteristics of high efficiency, convenience and strong adaptability. Common adsorbents are mainly divided into four categories: soils, biomasses, microorganisms and new composite materials [14]. Among them, most of the first three adsorbents are difficult to exert their advantages in a bad environment, while the last adsorbent is usually not affected by bad adsorption conditions. Therefore, the fourth kind of adsorbent has the most prospects. The commonly used adsorbents are synthetic resin [15], activated carbon [16], pure or composite silica (silica gel) [17,18], active Al_2O_3 [19–21], and so on. There are many new composite materials, for example, semiconductor nanocomposites [22], functionalized chitosan [23], ion-imprinted polymers [24], magnetic nanocomposites [25,26], metal-organic frameworks [27] and so on. All of them can absorb lanthanum ions, but only magnetic materials can be used conveniently because of their easy separation characteristics.

The purpose of this study is to study the adsorption efficiency of a new nano-material for rare-earth ions. First, a new adsorbent was developed, which could efficiently and selectively adsorb lanthanum ion (La(III)), and could be recycled. Second, we studied the effect of a single factor on the removal rate of La(III) without considering the interaction. Finally, the response surface methodology (RSM) was used to optimize the adsorption conditions and predict the experimental results.

2. Experimental methods

2.1. Reagents

Nanoscale magnetic oxide (Fe_3O_4) was purchased from Aladdin Reagent Shanghai Co., Ltd., (Fengxian District, Shanghai, China). Concentrated ammonia ($NH_3{\cdot}H_2O$) was purchased from Shanghai Jiuyi Chemical Reagent Co., Ltd., (Jinze Town, Qingpu District, Shanghai, China). Absolute ethanol (C_2H_6O) and methanol (CH_3OH) were purchased from Tianjin Hengxing Chemical Reagent Manufacturing Co., Ltd., (Dongli District, Tianjin, China). Ethyl orthosilicate ($C_8H_{20}O_4Si$, TEOS) was purchased from Xilong Chemical Co., Ltd., (Shantou, Guangdong Province, China). Lanthanum nitrate ($La(NO_3)_3{\cdot}6H_2O$) and gadolinium nitrate hexahydrate ($Gd(NO_3)_3{\cdot}6H_2O$) were purchased from Shanghai No. 1 Reagent Factory (Putuo District, Shanghai, China). Arsenazo III ($C_{22}H_{18}As_2N_4O_{14}S_2$) was purchased from Shanghai Debang Chemical Co., Ltd., (Jinshanwei Town, Jinshan District, Shanghai, China). Dichloromethane (CH_2Cl_2) was purchased from Changzhou Aohua Chemical Co., Ltd., (Zhonglou District, Jiangsu Province, China). Tris(2-aminoethyl)amine ($C_6H_{18}N_4$) was purchased from Hefei Geen Technology Co., Ltd. (Jinzhai Road, Shushan District, Hefei, Anhui Province, China) 3,4-dihydroxybenzaldehyde ($C_7H_6O_3$) was purchased from Wuhan Jiangmin Huatai Pharmaceutical Chemical Co., Ltd. All the above reagents were of analytical grade and were not further purified.

2.2. Characterization

The morphology and elemental composition of the material were determined by transmission electron microscope (TEM) and EDS (JEOL Ltd. (Haidian District, Beijing, P.R. China), JEM-2010(HR)). The phase of the material was determined by X-ray diffraction (XRD; DX-2700B, Dandong Haoyuan Instrument Co., Ltd., Dandong City, Liaoning Province, China). The functional groups of the material were determined by Fourier-transform infrared spectroscopy (FT-IR; Nicolet5700, American Thermoelectric Group, Pudong New Area, Shanghai, China).

2.3. Preparation of Fe_3O_4@SiO_2

The improved Stöber method was used for the synthesis of Fe_3O_4@SiO_2 particles [28]. One gram of Fe_3O_4 nanoparticles was dispersed in a mixed solution of 200 mL of ethanol, 40 mL of deionized water and 2.0 mL of concentrated aqueous ammonia solution (28 wt.%), and ultrasonically dispersed for 0.5 h to achieve uniform dispersion. Subsequently, 0.8 mL of tetraethyl orthosilicate solution was added dropwise during the stirring process, and the mixture was vigorously stirred at room temperature for 6 h. Finally, the silica-coated Fe_3O_4 nanoparticles were separated by a permanent magnet bar, washed three times with deionized water, and vacuum dried at 50°C for 12 h. The synthesis of Fe_3O_4@SiO_2 is shown in Fig. 1.

2.4. Synthesis of tripod ligands

60 mL of dichloromethane and 60 mL of methanol solution were mixed in a beaker, and 1.66 g of 3,4-dihydroxybenzaldehyde was added. Then the beaker was

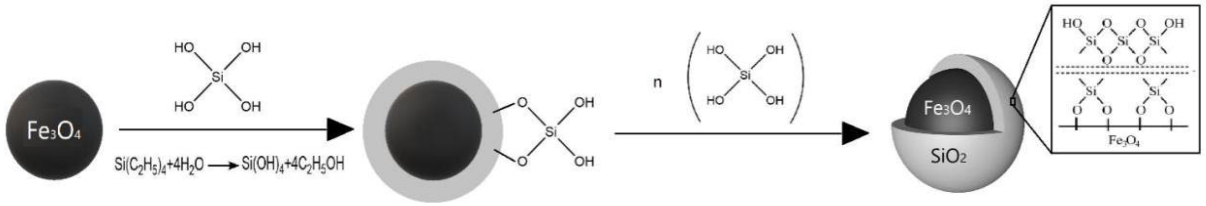

Fig. 1. Synthesis method of Fe_3O_4@SiO_2.

placed on a magnetic stirrer. 4 mL of dichloromethane solution containing 0.58 mL of tris(2-aminoethyl)amine were added dropwise during the stirring. After completion of the dropwise addition, stirring was continued for 5 h at room temperature. Then a yellow precipitate was formed, suction filtered, washed with an ethanol solution, and dried for use. The synthesis of the tripod ligand is shown in Fig. 2.

2.5. Synthesis of magnetic tripod ligands

One gram of the obtained Fe_3O_4@SiO_2 was weighed into a 250 mL Erlenmeyer flask, and 1.5 g of tripod ligand and 80 mL of ethanol solution were added to it. The mixture was shaken in a water bath at 25°C for 6 h. Solid–liquid separation using permanent magnets. After that, the solid matter was washed three times and dried under vacuum at 50°C for 12 h to obtain a magnetic tripod ligand. The synthesis of the magnetic tripod ligand is shown in Fig. 3.

2.6. Adsorption experiment of rare-earth ions

According to the report of Yan-jie et al. [29], the residual La(III) ion concentration in the solution was determined by arsenazo III spectrophotometry. Gd(III) was determined by EDTA titration [30,31]. Calculate the removal rate R and adsorption amount Q_t of La(III) by magnetic tripod ligand adsorbent by using Eqs. (1) and (2), respectively.

$$R = \frac{C_0 - C}{C_0} \times 100\% \tag{1}$$

$$Q_t = \frac{(C_0 - C) \times V}{m} \tag{2}$$

where C_0 and C are the concentrations of La(III) before and after adsorption, respectively (mg/L). V is the volume of the La(III) solution (L), m is the mass of the adsorbent (g).

The adsorption process of La(III) can be inferred from the adsorption isotherm model and the adsorption kinetic model. The commonly used adsorption isotherm models are *L*-type (Langmuir adsorption isotherm model) and *F*-type (Freundlich adsorption isotherm model). The *L*-type and the *F*-type are shown in Eqs. (3) and (4), respectively.

$$Q_t = \frac{bQ_{\max}C_t}{1 + bC_t} \Rightarrow \frac{C_t}{Q_t} = \frac{1}{bQ_{\max}} + \frac{1}{Q_{\max}}C_t \tag{3}$$

$$Q_t = kC_t^{\frac{1}{n}} \Rightarrow \ln Q_t = \ln k + \frac{1}{n}\ln C_t \tag{4}$$

where C_t is the concentration of La(III) at each point on the concentration-adsorption capacity curve (mg/L); b is the adsorption constant; $Q_{\max}$ is the maximum adsorption capacity (mg/g); k is a constant representing the adsorptive ability of adsorbents; $1/n$ is a constant for judging the difficulty of adsorption.

The commonly used dynamic models are the pseudo-first-order model and pseudo-second-order model. Their formulas are as follows:

$$\ln(Q_e - Q_t) = \ln Q_e - k_1 t \tag{5}$$

$$\frac{t}{Q_t} = \frac{1}{k_2 Q_e^2} + \frac{1}{Q_e}t \tag{6}$$

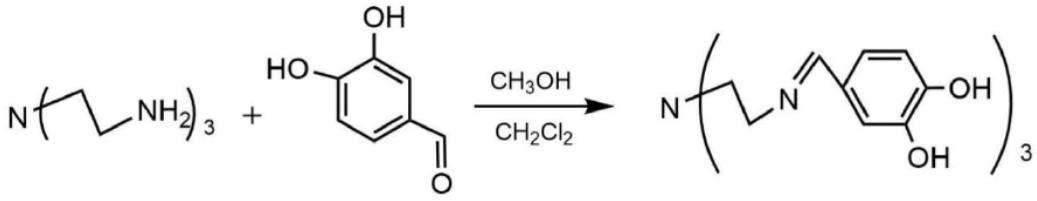

Fig. 2. Synthesis method of tripod ligand.

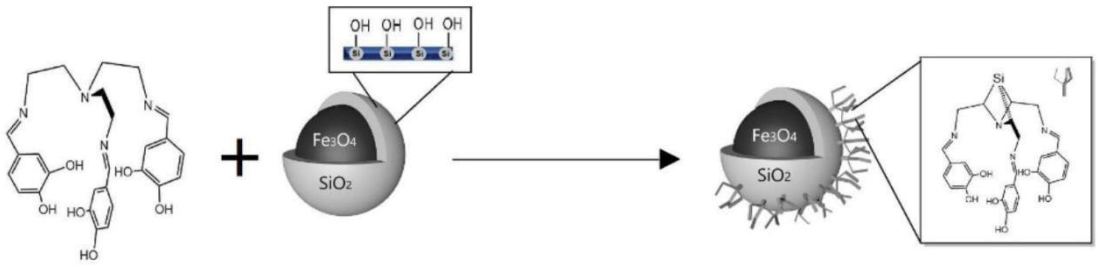

Fig. 3. Synthetic principle of magnetic tripod ligand.

where Q_e is the amount of adsorption when the adsorption process reaches an equilibrium state (mg/g); t is adsorption time (min).

3. Result

3.1. TEM analysis

The morphology of the Fe_3O_4, Fe_3O_4@SiO_2 and magnetic tripod ligands is shown in Fig. 4. By comparing Figs. 4a and b, it can be found that a very thin layer of material is wrapped around the outside of Fe_3O_4 and is SiO_2. Type and content of elements on the outside of Fe_3O_4@SiO_2 were analyzed by EDS and exhibited in Figs. 4c and d. The results showed that there were C, O, Si, Fe and Cu elements in the specified area. Moreover, it was believed that the most likely external substances of Fe_3O_4 were amorphous SiO_2 and tripod ligands. However, due to the large interference of background elements in the measurement process, it is difficult to determine that the tripod ligand must exist. Based on the weight percentage of the element and the atomic percentage, it was believed that amorphous silica must exist and it was very likely to share a certain amount of oxygen atoms with Fe_3O_4 [32].

3.2. XRD analysis

Compared with standard PDF cards, Fig. 5a data of the diagram are consistent with JCPDS No.75-0033. The position at which the diffraction peak appears from strong to weak was 2θ = 35.5°, 62.6°, 30.1°, 57.0°, 43.1°. Combined with the crystal plane parameters, it can be judged that there are cubic Fe_3O_4 in both materials. Also, in Fig. 5b, there is a weaker diffraction peak in the range of 2θ = 18°–25°, and the peak is judged to be the peak of amorphous silica [33], but in Fig. 5a, it is not shown that a similar peak appears. So SiO_2 was successfully wrapped on the surface of the Fe_3O_4, which provided conditions for the next step of attaching the tripod ligand to the surface of SiO_2.

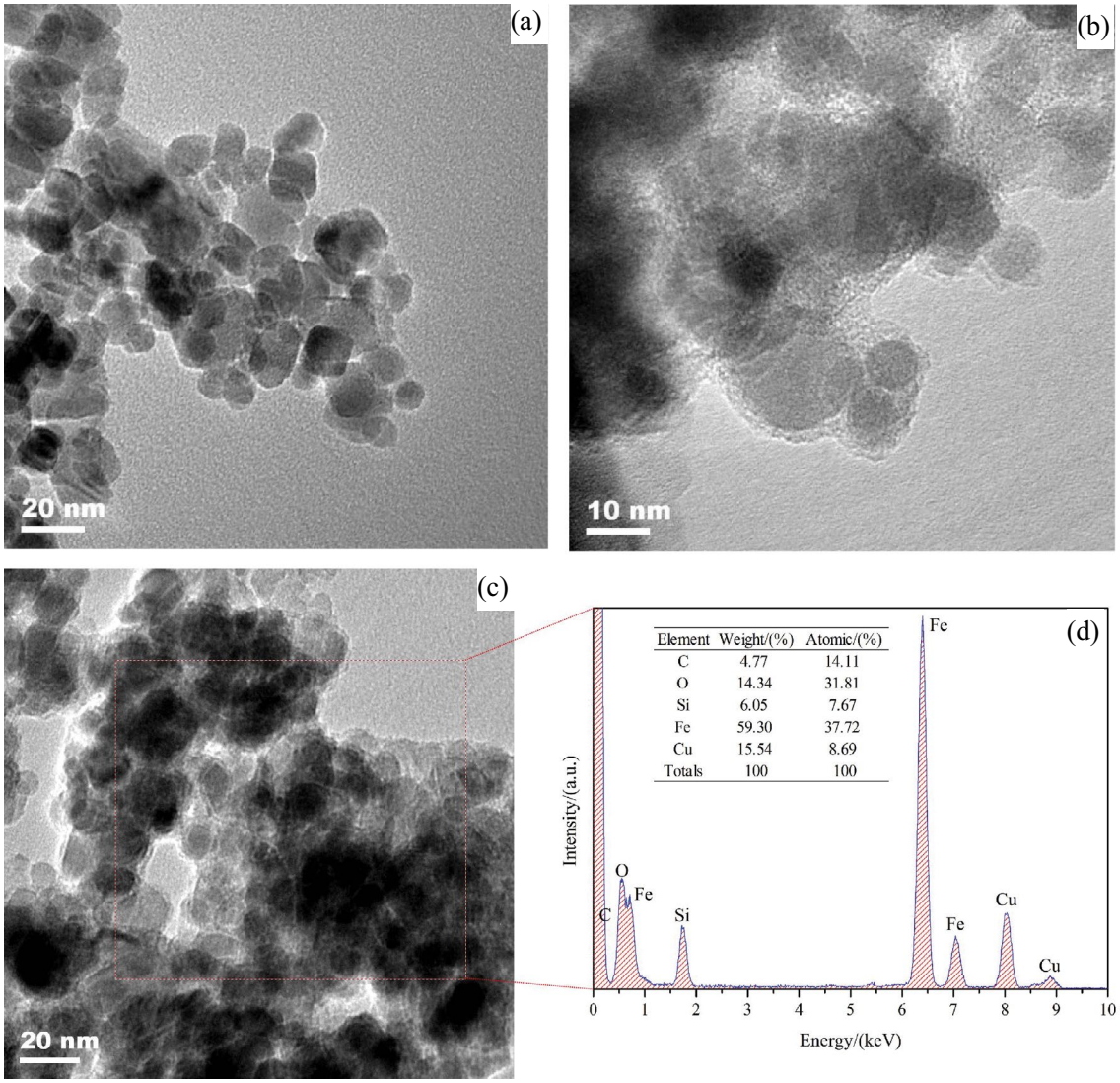

Fig. 4. TEM images of (a) Fe_3O_4, (b) Fe_3O_4@SiO_2 and (c) magnetic tripod ligand. (d) EDS analysis image of magnetic tripod ligand.

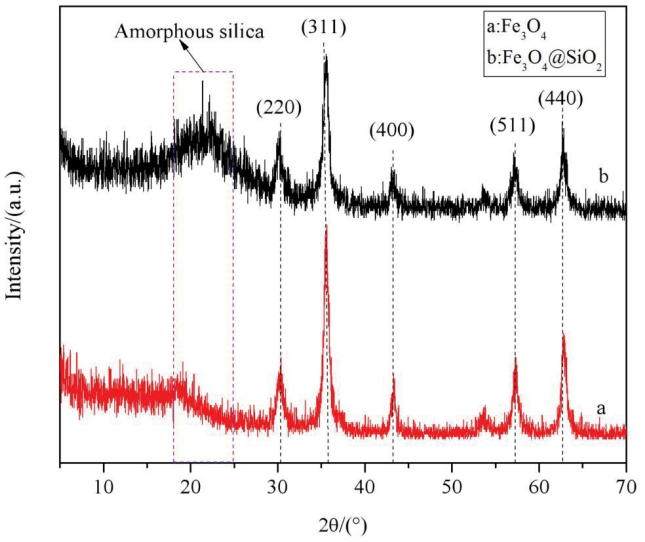

Fig. 5. X-ray diffraction diagram of Fe_3O_4 (a) and Fe_3O_4@SiO_2 (b).

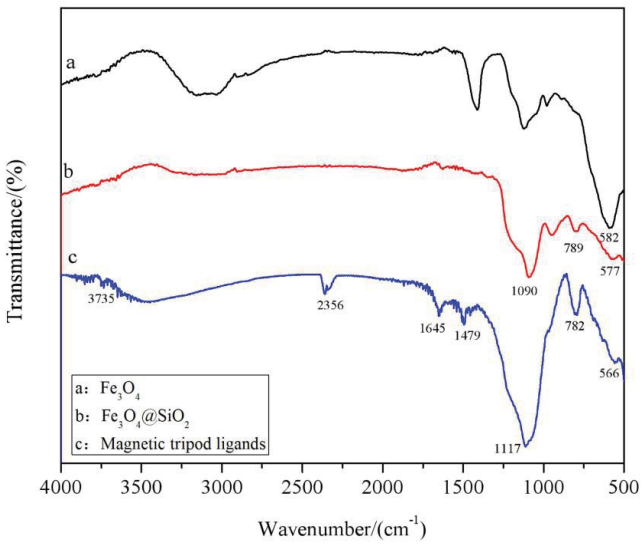

Fig. 6. Diagram of the infrared spectra of Fe_3O_4 (a), Fe_3O_4@SiO_2 (b) and Magnetic tripod ligand (c).

3.3. FT-IR analysis

In Fig. 6a the absorption peak at 582 cm^{-1} corresponded to the stretching vibration of Fe-O of Fe_3O_4. Fe-O characteristic peak of Fe_3O_4 coated with SiO_2 was moved from 582 to 577 cm^{-1} and 566 cm^{-1} in (b) and (c), respectively [34]. It shows that a "redshift" has occurred. The strong and broad absorption peak near 1,090 cm^{-1} in (b) and 1,117 cm^{-1} in (c) are the anti-symmetric stretching vibration absorption peaks of Si–O–Si [35]. The absorption peaks at 789 cm^{-1} in (b) and 782 cm^{-1} in (c) are the symmetric stretching vibration peaks and bending vibration peaks of Si–O–Si, respectively. It confirms that SiO_2 is successfully coated on the surface of Fe_3O_4 again.

In Fig. 6c, the wave number exhibited ν(C=N) stretching at 1,645 cm^{-1} and the vibration with a wave number of 1,479 cm^{-1} is caused by the aromatic ring [36]. A wide, irregular double peak appeared near 2,356 cm^{-1}, perhaps caused by CO_2 in the air. Several broad and small peaks near 3,735 cm^{-1} may be the absorption peaks of hydroxyl groups. In summary, the tripod ligands are successfully grafted on the surface of Fe_3O_4@SiO_2.

3.4. Effect of adsorbent dosage on adsorption

In this work, 50 mL of 50 mg/L La(III) solution in a Erlenmeyer flask received 10, 20, 30, 40, 50, 60, 70, 80 or 90 mg of adsorbent, respectively. The flask was placed in the oscillator. After shaking at 25°C for 2 h, the adsorbent was separated by a permanent magnet, and the supernatant was filtered through a 0.45 μm filter for the measurement of the residual concentration. Thereby, the La(III) removal rate was calculated. The experimental results are shown in Fig. 7.

As shown in Fig. 7, when the initial concentration of La(III) in the solution is fixed, the La(III) adsorption rate initially increases rapidly as the dosage increases. With the extension of time, the increase of adsorption rate tends to be stable, and the adsorption rate is close to 100%. When the dosage is increased from 10 to 80 mg, the adsorption rate of La(III) increases from 78.7% to 99.5%, while the adsorption

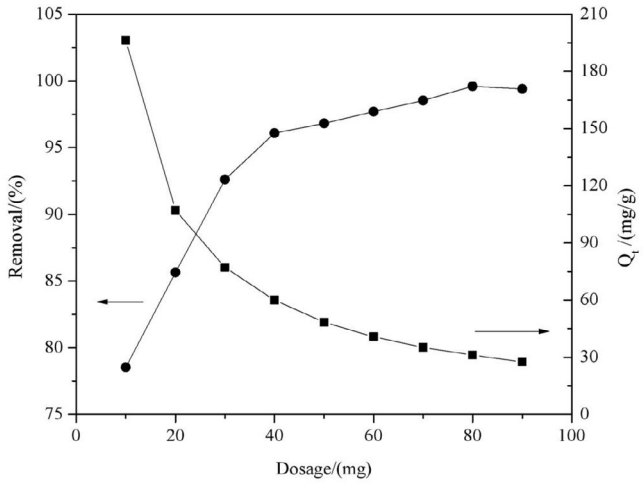

Fig. 7. Effect of dosage of adsorbent.

amount of La(III) decreases from 197.3 to 22.6 mg/g. It shows that the appropriate increase in dosage can effectively increase the removal rate of La(III). Because the amount of adsorbent directly affects the cost of recovering La(III), it is possible to save cost by selecting the appropriate dosage on the premise of ensuring higher recovery. In this study, 80 mg is chosen as the optimum dosage due to the highest adsorption rate.

3.5. Effect of adsorption time on adsorption

Eight sets of 50 mL of La(III) solution with a concentration of 50 mg/L were added to the Erlenmeyer flasks. After adding 80 mg of the adsorbent, respectively, the adsorption test was carried out at 25°C with a constant temperature oscillator, and the adsorption times were 5, 10, 20, 30, 60, 90, 120, 150 min, respectively. After solid–liquid separation using a permanent magnet, the supernatant was removed,

and then the absorbance was measured, and the removal rate was calculated. The experimental results are shown in Fig. 8.

When the adsorption time was 30 min, the removal rate of La(III) could reach 90.6%. With the extension of time, the adsorption rate of La(III) continues to increase and gradually reaches equilibrium. In the initial stage, the adsorption rate is faster, probably due to a large number of available adsorption sites in the adsorbent, and gradually decreases as the adsorption site is occupied by La(III), so that the adsorption rate becomes slow until the adsorption equilibrium is reached. Therefore, when the equilibrium state of adsorption and desorption is not reached, appropriately prolonging the adsorption time is advantageous for increasing the removal rate of La(III).

However, as the adsorption time is prolonged, the adsorption rate would decline, and the treatment cycle would be prolonged, which could increase the operating cost. Thus, it is necessary to comprehensively consider the treatment effect and economic benefits to select the appropriate adsorption time. In this study, we chose the optimum adsorption time of 120 min, because the adsorption rate reached the highest (96.5%).

3.6. Effect of interfering ions on adsorption

Seven groups of La(III) solutions containing Gd(III) concentrations of 0, 10, 30, 50, 80, 100, 120 mg/L, respectively, were prepared in 50 mL of Erlenmeyer flasks with a La(III) concentration of 30 mg/L. After adding 80 mg of the adsorbent, respectively, the adsorption test was carried out at 25°C for 2 h with a constant temperature oscillator, followed by solid–liquid separation with a permanent magnet, and then the supernatant was removed and filtered through a 0.45 μm filter. Residual La(III) concentration was measured, and the removal rate was calculated.

The experimental results are shown in Fig. 9. With the increase of Gd(III) concentration, the removal rate of La(III) by the adsorbent decreased, but the decrease rate was not large, and the removal rate decreased by 6.9%. When the concentration of Gd(III) was increased to 50 mg/L, the removal rate decreased by 1.2 percentage points. The latest figure indicates that the removal rate of La(III) is not substantially affected. Moreover, when the concentration of Gd(III) exceeded 50 mg/L, the removal rate decreased rapidly. It indicates that excessive Gd(III) concentration inhibits the removal rate of La(III) by the adsorbent, probably because the high concentration of Gd(III) reduces the contact probability of La(III) with the adsorption site on the adsorbent surface. All in all, the removal rate of La(III) by adsorbent was not affected by interference ion Gd(III), and the adsorbent could selectively adsorb La(III).

3.7. Effect of solution pH on adsorption

Seven groups of 50 mL of La(III) solution with a concentration of 50 mg/L were added to the Erlenmeyer flasks, and the pH of the solution was adjusted to 1, 2, 3, 4, 5, 6 or 7, respectively. After adding 80 mg of adsorbent, respectively, it was adsorbed in a constant temperature oscillator at 25°C for 2 h. The solid–liquid separation was carried out with a permanent magnet, and then the supernatant was removed and filtered with a 0.45 μm filter. Residual La(III) concentration was measured, and the removal rate was calculated.

In this study, the magnetic tripod ligand was an adsorbent with a ligand. The pH of the solution is one of the most important factors affecting coordination. It can not only affect the existence of La(III) in solution but also affect the coordination characteristics of the ligand itself, such as the electronic effect of the functional group. In particular, in the process of recovering rare earth elements in waste, the leachate is often acidic, and the pH is generally low, so the effect of the adsorbent on the adsorption of La(III) is not investigated when pH > 7. The experimental results are shown in Fig. 10.

When pH < 5, the removal rate of La(III) increases with the increase of pH, which is probably because the phenolic hydroxyl groups on the three branches of the tripod ligand form a complex with La(III) to achieve the adsorption effect. When the pH is very low, the H^+ concentration in the solution is very high, and the phenolic hydroxyl group is difficult to ionize H^+, and it is

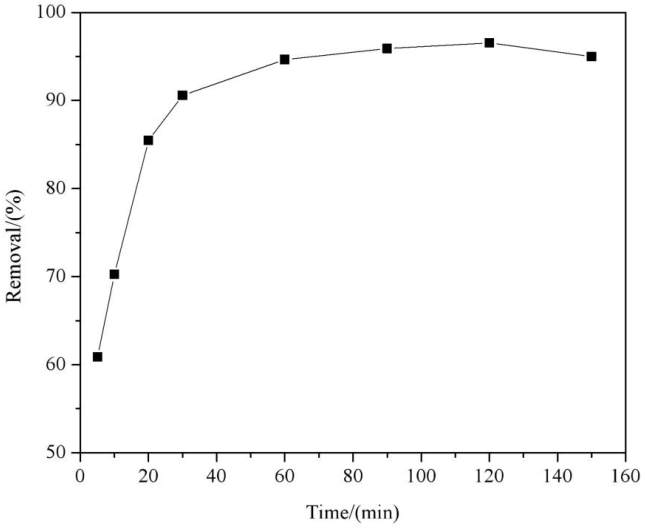

Fig. 8. Effect of adsorption time.

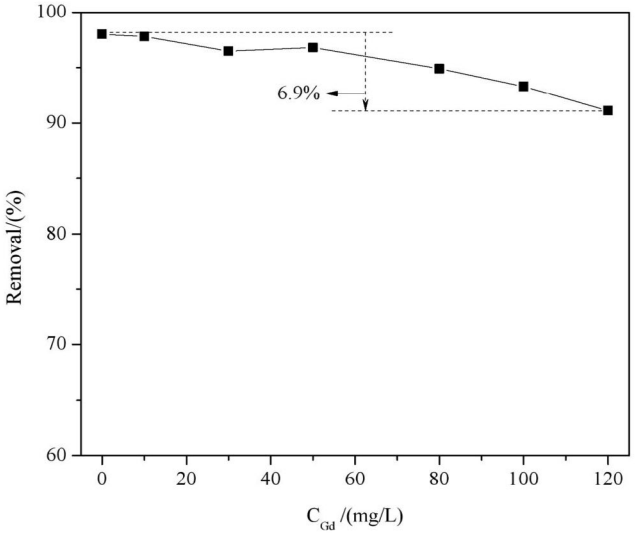

Fig. 9. Effect of interfering ions.

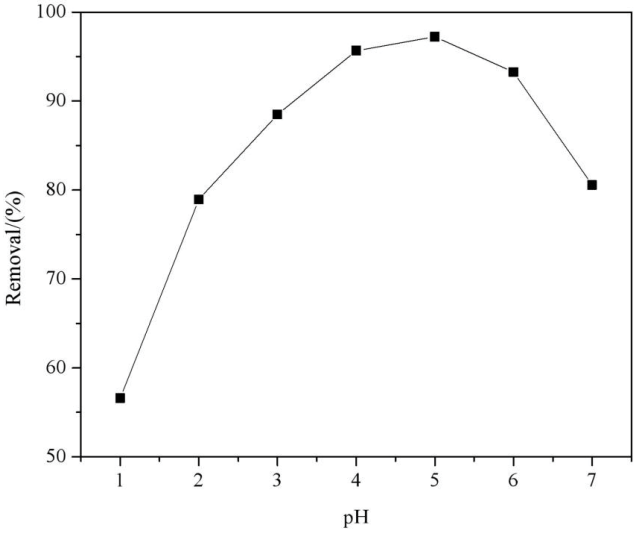

Fig. 10. Effect of pH value.

difficult to form coordination sites. Therefore, too little pH will affect the adsorption effect. Also, as the pH increases, the phenolic hydroxyl group can provide more coordination sites, and the adsorption effect gets the better of them. When pH = 5.0–7.0, the removal rate of La(III) decreased, and when pH = 7.0, the removal rate was only 80.56%. So pH = 5 was chosen as the optimum experimental condition. Perhaps the hydroxyl group on the adsorbent is a Lewis base, and La(III) is a typical Lewis acid. According to the Lewis acid-base theory, when the pH increases, the coordination of the ligand with the rare earth ions is inhibited, which affects the adsorption effect [37].

3.8. Response surface methodology

3.8.1. Experimental design of RSM

A three-factor and three-level Box–Behnken design (BBD) was adopted (16 runs, four centre points) so as to establish a suitable adsorption model. The impact factors and levels in the experiment are shown in Table 1.

The functional relationship between these factors was fitted by a quadratic polynomial as follows:

$$Y = \beta_0 + \beta_1 X_1 + \beta_2 X_2 + \beta_3 X_3 + \beta_{12} X_1 X_2 + \beta_{13} X_1 X_3 + \beta_{23} X_2 X_3 + \beta_{11} X_1^2 + \beta_{22} X_2^2 + \beta_{33} X_3^2 \quad (7)$$

where Y is the response variable (removal, %); β_0 is the model constant; β_1, β_2, β_3 are coefficients of linear; β_{11}, β_{22}, β_{33} are coefficients of quadratic, and β_{12}, β_{13}, β_{23} are coefficients of the interaction term, respectively. Moreover, the model was evaluated and optimized using ANOVA.

The experiments were carried out according to the operating plan given by the Design-Expert (Version 7.0). The experimental values were also recorded and are shown in Table 2.

In Table 3, for the adjusted *R*-squared and standard deviation, the Quadratic and Cubic models are more able to describe experimental data, but compared with the Cubic model, Quadratic's sequential model has a smaller *p*-value and reaches a significant level. Therefore, the Quadratic model was selected and analyzed for the variance.

Table 1
Factors and levels selection

Factors	Unit	Coded factors	Level		
			–1	0	1
Dosage	mg	$X_1 = A$	40	60	80
Time	min	$X_2 = B$	30	65	100
pH	–	$X_3 = C$	3	4	5

Table 2
Response values and model predictions observed in different combinations

Run	Value of coded variables			Removal/(%)(La^{3+})	
	A	*B*	*C*	Actual	Predicted
1	–1	–1	0	68.54	69.06
2	1	–1	0	75.4	74.42
3	–1	1	0	90.12	91.17
4	1	1	0	97.54	97.08
5	–1	0	–1	72.01	72.01
6	1	0	–1	82.95	84.45
7	–1	0	1	83.98	82.55
8	1	0	1	81.29	81.36
9	0	–1	–1	73.35	72.86
10	0	1	–1	91.28	90.27
11	0	–1	1	70.66	71.60
12	0	1	1	98.56	98.98
13	0	0	0	78.95	79.60
14	0	0	0	80.14	79.60
15	0	0	0	79.56	79.60
16	0	0	0	79.89	79.60

3.8.2. Establishment of the quadratic polynomial regression equation

After rejecting source A^2 that has a negative effect but has no significant effect on the removal rate, the final equation in terms of coded factors as follows:

$$Y(\%) = 79.60 + 2.82A + 11.19B + 1.86C + 0.14AB - 3.41AC + 2.49BC + 3.33B^2 + 0.49C^2 \quad (8)$$

The predicted values of the improved model for the experimental data are shown in Table 2. The improved ANONA results are shown in Table 4. In the improved model (Eq. (8)), the "Sum of Squares" of residuals was reduced and the lack of fit was non-significant, which indicated that the model and the experimental data were well simulated.

The original experimental data were predicted according to Eq. (8), and the predicted results are shown in Table 2. The difference between the predicted value and the actual value

Table 3
Test of four models

Source	Std. dev.	*R*-Squared	Adjusted *R*-Squared	Predicted *R*-Squared	PRESS	Sequential *p*-value	
Linear	3.25	0.8961	0.8701	0.7921	253.77	<0.0001	
Interaction	2.48	0.9546	0.9243	0.8125	228.83	0.0501	
Quadratic	1.29	0.9918	0.9795	0.8783	148.48	0.0119	Suggested
Cubic	0.51	0.9993	0.9967	/	/	0.0372	Aliased

Table 4
Main effects and interaction effects of improved ANOVA

Source	Sum of Squares	*df*	Mean Square	*F* Value	*p*-value Prob. > *F*	Yes or No significant
Model	1,210.43	8	151.3	105.85	<0.0001	Y(Yes)
A-Dosage	63.45	1	63.45	44.39	0.0003	Y
B-Time	1,002.4	1	1,002.4	701.26	<0.0001	Y
C-pH	27.75	1	27.75	19.41	0.0031	Y
AB	0.078	1	0.078	0.055	0.8215	N(No)
AC	46.44	1	46.44	32.49	0.0007	Y
BC	24.85	1	24.85	17.38	0.0042	Y
B^2	44.49	1	44.49	31.12	0.0008	Y
C^2	0.97	1	0.97	0.68	0.4372	N
Residual	10.01	7	1.43			
Lack of Fit	9.21	4	2.3	8.69	0.0533	N
Pure Error	0.79	3	0.26			
Cor. Total	1,220.44	15				
Std. Dev.	1.20		*R*-Squared		0.9918	
Mean	81.51		Adj. *R*-Squared		0.9824	
C.V. (%)	1.47		Pred. *R*-Squared		0.9218	
PRESS	95.48		Adeq. Precision		33.358	

is described in Fig. 11. It can be seen from Fig. 11a that the predicted values are almost identical to the actual values, and they are all approximately on the same line. As can be seen from Fig. 11b, the internally studentized residual shows a linear relationship with the normality probability, which indicates that the residual is consistent with the normal distribution. In Fig. 11c the absolute value of the largest residual value appears in the 6th and 7th processing groups, both of which are greater than 2. The absolute value of the smallest residual value appears in the 5th, 8th and 15th processing groups, which are close to 0. In summary, the second-order polynomial model, Eq. (8), provides a good quantitative description of the experimental results.

3.8.3. Response surface diagram and its analysis

The response surface curve is shown in Fig. 12. When pH = 4.00, the removal rate of La(III) increases with the increase of dosage and time, and wherein the dosage has little effect on the removal rate, as shown in Fig. 12a. When time = 65.00 min, the removal rate of La(III) increases with the increase of dosage and pH, but the removal rate is only increased by a small margin, as shown in Fig. 12b. When dosage = 60.00 mg, the removal rate of La(III) increases with time and pH, where pH has little effect on the removal rate, as shown in Fig. 12c. All in all, the prolongation of adsorption time is of great benefit for the improvement of La(III) removal rate.

3.8.4. Establishment of the optimal solution

To maximize the La(III) removal rate, we further determined the optimal experimental parameters by the established second-order polynomial model. The specific parameters are shown in Fig. 13.

In Fig. 13, the optimum experimental conditions are dosage = 40 mg, time = 100 min, pH = 5, at which time the

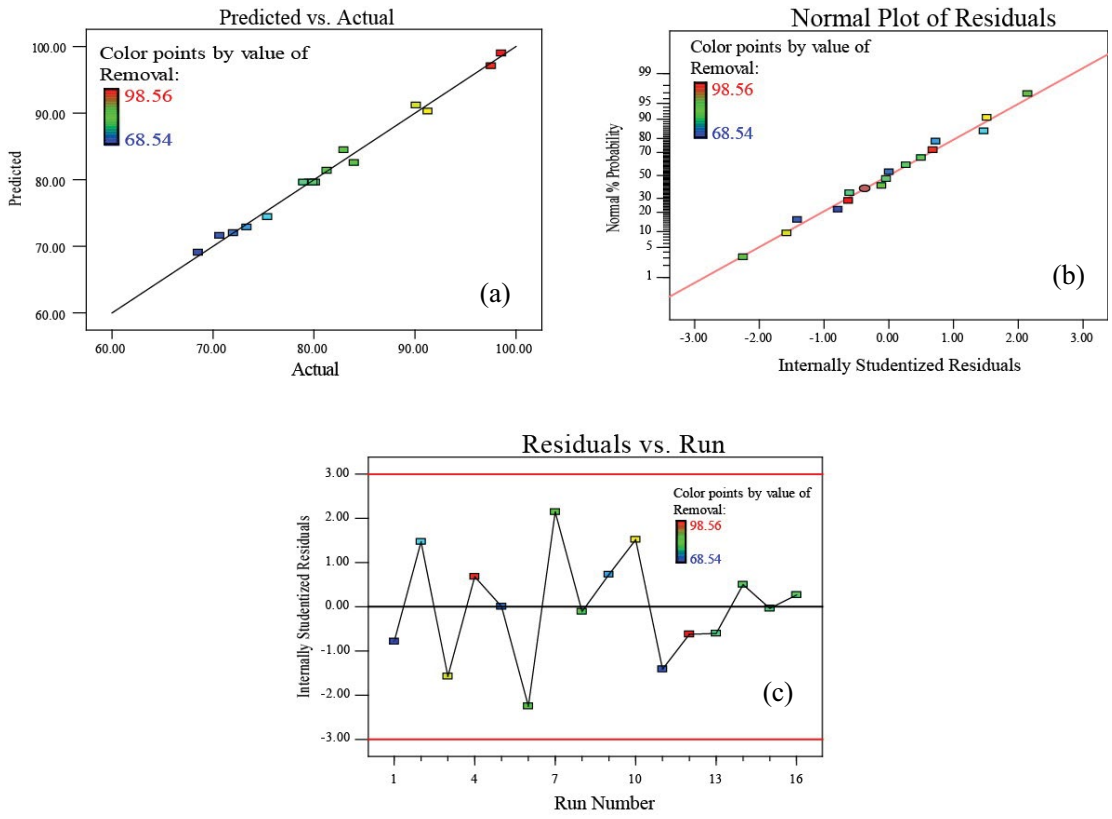

Fig. 11. A graph of the actual response values vs. the predicted response values (a); normal probability plot (b); the plot of the residuals vs. the experimental run order (c).

removal rate can reach up to 99.42%. This ideal situation is about 98.2% desirable to meet expectations. The relevant statistics of the predicted values are shown in Table 5.

By summarizing the application of the RSM in the removal of pollutants by adsorbents in recent years, we found that the quadratic polynomial model established by the central composite design (CCD) method, CCRD (central composite rotatable design) or the BBD method can well predict the experimental results as shown in Table 6 [38–47]. Many researchers have carried out verification experiments on the prediction results. We found that the predicted values under optimal operating conditions are very close to the actual values and always slightly higher than the actual values. And the experimental results showed that the removal rate of La(III) could reach 97.9%.

3.9. Adsorption and regeneration of magnetic tripod ligands

The already adsorbed La(III) was removed from the adsorbent by using a 0.5 mol/L NaOH solution, and then the adsorbent could be restored to the initial state again after elution. 50 mg of the adsorbent was added to 100 mL of 100 mg/L La(III) solution, and the adsorption equilibrium was achieved after 120 min of adsorption. After the solid–liquid separation, the adsorption/desorption test was carried out for five cycles. The experimental results are shown in Fig. 14. After the adsorbent was used for two cycles, the removal rate of La(III) by the adsorbent was reduced to 94.20% of the first cycle. After five times of use of the adsorbent, the removal rate decreased to 78% compared with the initial adsorbent effect. The process of adsorbent recycling is shown in Fig. 15.

3.10. Adsorption thermodynamics and kinetic model of La(III)

It can be seen that the adsorption process is more accordance with the *F*-type and pseudo-second-order kinetic model from Figs. 16, 17 and R^2 in Table 7. The results showed: (1) the surface of adsorbent was not uniform; (2) the adsorption process was a chemical adsorption process. Thereinto, $0.1 < 1/n < 0.5$ indicated that the chemical adsorption process was very easy to occur. When the specific adsorption conditions were met, the equilibrium adsorption amount could reach 30.5997 mg/g. By comparing the adsorption amount of different adsorbents for lanthanum ions, it can be seen that the adsorbent in this study has a higher adsorption capacity for lanthanum ions. And the maximum adsorption capacity can reach 61.19 mg/g. Moreover, it is easy to see from Table 8 [48–57] that most for the adsorption type are *L*-type. And their dynamic models all conform to the pseudo-second-order model.

3.11. Mechanism analysis of selective adsorption of La(III)

The adsorption of La(III) by adsorbent is mainly coordination chelation, so the possible mechanism of selective adsorption of La(III) is worthy of discussion. In most rare earth complexes, the chemical bond between the central ion

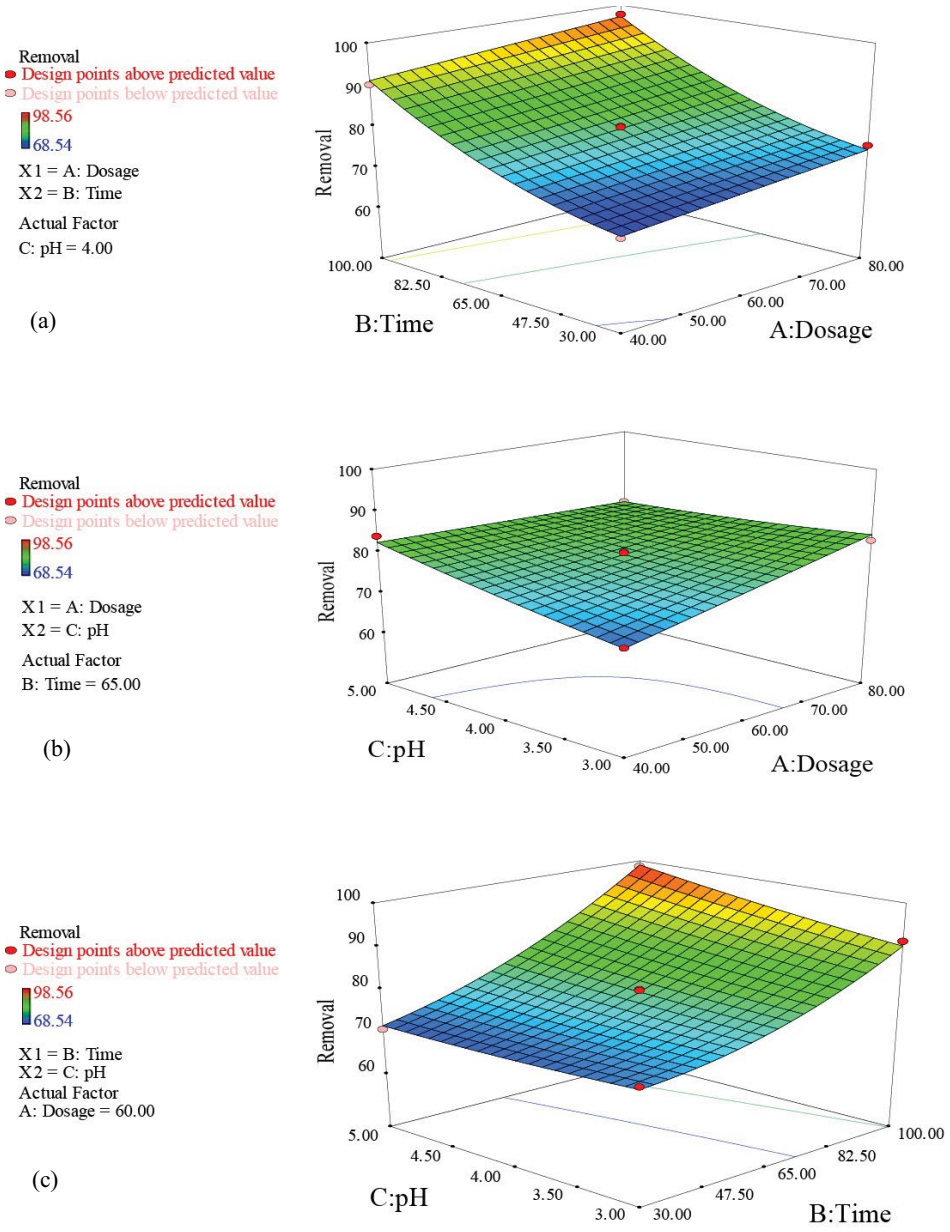

Fig. 12. Two-factor interaction diagram, interaction between *A* and *B* when pH = 4.00 (a); interaction between *A* and *C* when Time = 65.00 min; interaction between *B* and *C* when dosage = 60.00 mg.

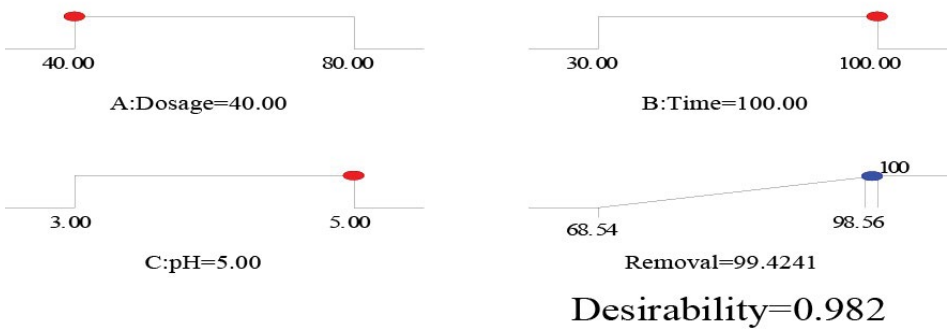

Fig. 13. Optimal solution of experimental parameters.

Table 5
Statistics of model predictions

Response	Prediction	SE Mean	Confidence interval (CI)		SE Pred.	Prediction interval (PI)	
			95% CI low	95% CI high		95% PI low	95% PI high
Removal(%)	99.42	1.37	96.19	102.66	1.82	95.13	103.72

Table 6
RSM for prediction of removal rate

Adsorbent	RSM type	Predicted value/(%)	Measured value/(%)	Ref.
Na-Bentonite	CCD	95.30	94.30	[38]
NaP:HAp nanocomposite	BBD	97.45	96.30	[39]
Zeolite by calcination	CCRD	82.20	80.00	[40]
Brushite	BBD	90.83	88.78	[41]
Cu@Mn-ZnS-NPs-AC	CCD	99.80	98.90	[42]
MNPs	CCD	89.20	86.90	[43]
NH_2-MCM-41	CCD	79.79	75.60	[44]
Modified Litchi Pericarp	BBD	99.97	99.89	[45]
Activated carbon	CCD	100.00	99.00	[46]
MFA	BBD	100.00	98.00	[47]

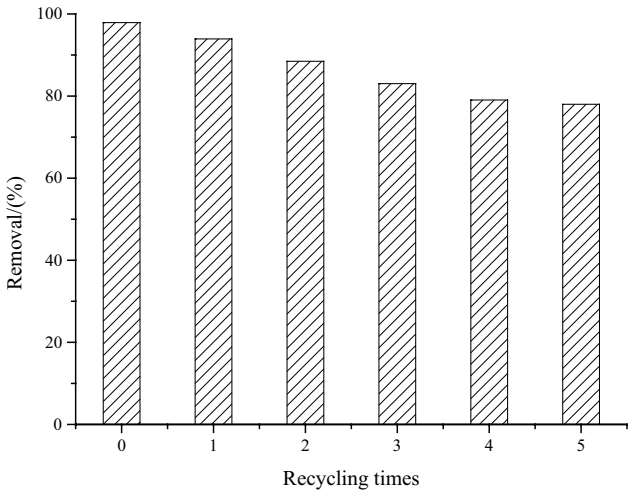

Fig. 14. Relationship between adsorbent recycling times and the removal rate.

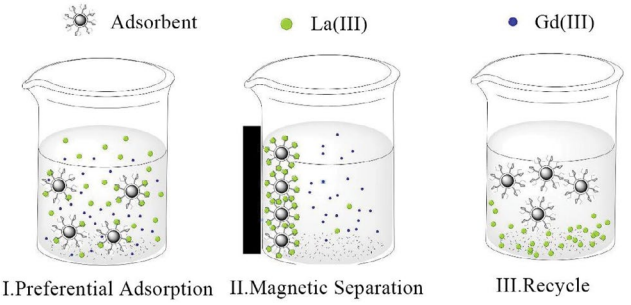

Fig. 15. Behavioral mechanism of selective adsorption of La(III) by adsorbents.

and the ligand is predominantly ionic. Therefore, the greater the electronegativity of the ligand atom of the ligand, the greater the coordination ability and the more stable the complex formed [47].

In general, as the ionic radius of the lanthanide element decreases, the coordination number tends to decrease, that is, the coordination number of the heavy rare earth element is less than that of the light rare earth element. The radius of La(III) is 106.1 pm, which is larger than that of Gd(III) that is 93.8 pm. For example, $[Ln(en)_4NO_3](NO_3)_2$, where Ln is La to Sm, the coordination number is 10; $[Ln(en)_4](NO_3)_3$, where Ln is Eu to Yb, and the coordination number is 8 [58].

On the one hand, the tripod ligand is a multidentate ligand that can coordinate with rare-earth ions. On the other hand, the tripod ligand has a special spatial structure, and the three branches can be rotated to capture specific central ions. Also, when the rare earth ions are used as the central ion, generally, the coordination number of the rare earth ions is large, and the coordination number is greater than 6, and it is obvious that the multidentate ligand forms a complex with the rare-earth ions. According to Liu et al.'s [59] research, we infer that the coordination number of lanthanum ion with tripod ligand is six. The structure of the complex is shown in Fig. 18. Other than that, the phenomenon of lanthanide contraction leads to a decrease in the coordination number [60], so the tripod ligand selectively captures rare-earth ions under various conditions. The magnetic tripod ligand not only has

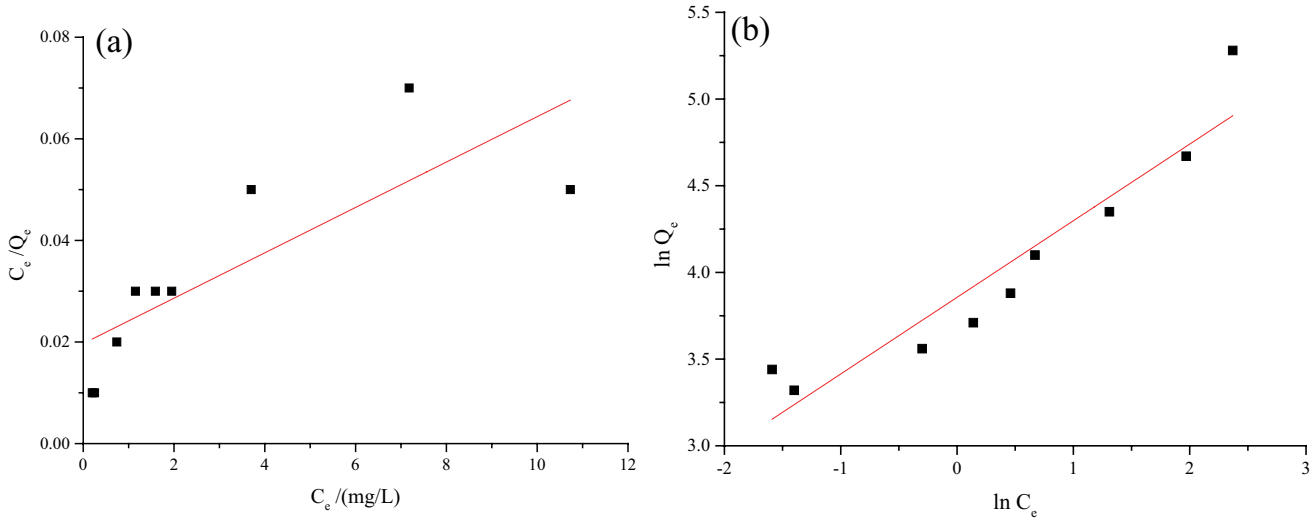

Fig. 16. *L*-type (a) and *F*-type (b).

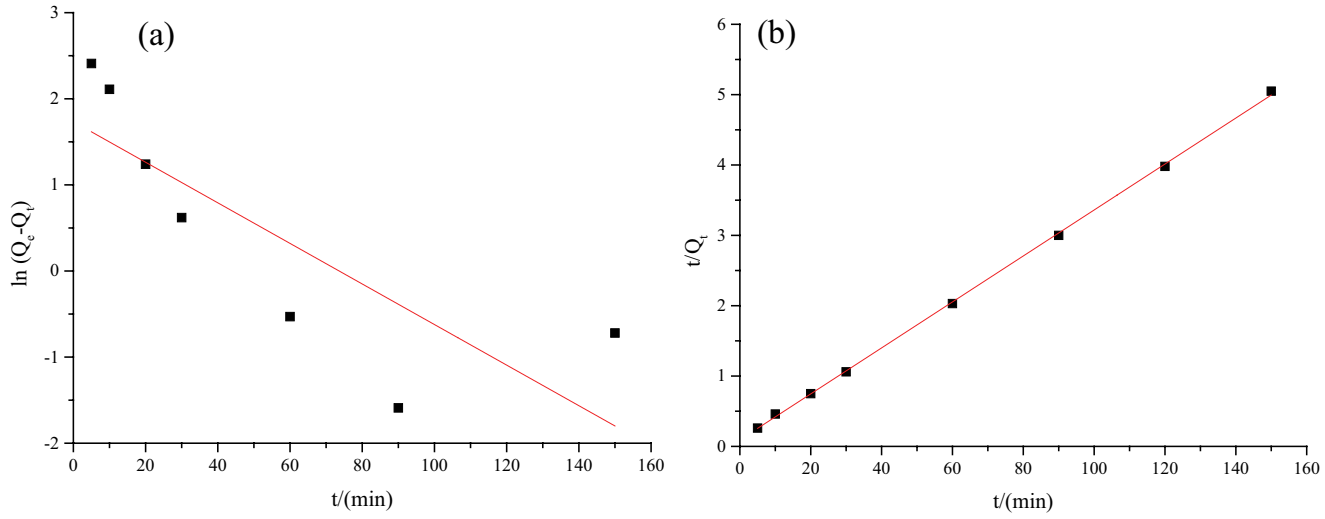

Fig. 17. Pseudo-first-order model (a) and Pseudo-second-order model (b).

Table 7
Thermodynamic and kinetic parameters were calculated from the formulas

L-type			F-type		
R^2	b (L/mg)	Q_{max} (mg/g)	R^2	1/n	k (L/mg)
0.6530	0.227	223.71	0.8944	0.4419	3.8562
Pseudo-first-order			Pseudo-second-order		
R^2	k_1 (g/mg·min)	Q_e (mg/g)	R^2	k_2 (g/mg·min)	Q_e (mg/g)
0.6714	0.0236	5.6644	0.9996	0.0115	30.5997

P.S.: R^2 is the square value of Pearson's correlation coefficient.

Table 8
Comparison of the adsorptive capabilities of different adsorbents for lanthanum ions

Adsorbents	REEs	Isotherm models	Kinetic models	Maximum adsorption capacity (mg/g)	References
Magnetic tripod ligand	La^{3+}	F	Ps2	61.19	This Study
Pleurotus ostreatus basidiocarps	La^{3+}	L	–	54.54	[48]
Stichococcus bacillaris	La^{3+}	L	Ps2	51.02	[49]
EDTA-β-cyclodextrin	La^{3+}	L	Ps2	47.78	[50]
CLN/SiO_2	La^{3+}	L	Ps2	29.48	[51]
GO-$CZ_{9:1}$	La^{3+}	–	–	17.29	[52]
Cys@CHI-magnetic	La^{3+}	L	Ps2	17	[53]
Bone powder	La^{3+}	L	–	8.7	[54]
HESI-SBA-15	La^{3+}	–	Ps2	8.23	[55]
Kaolinite	La^{3+}	L	Ps2	3.19	[56]
Hydroxyapatite	La^{3+}	F	Ps2	0.94	[57]

P.S.: F is Freundlich;
L is Langmuir;
Ps2 is Pseudo-second-order;
CLN/SiO_2 is cellulose-based silica modified by H_2SO_4;
GO-$CZ_{9:1}$ is three-dimensional graphene oxide-based-corn zein composites with mass ratio of 9:1;
Cys@CHI-magnetic is cysteine-functionalized chitosan magnetic nano-based particles.
HESI-SBA-15 is a novel modified SBA-15 with covalently bonded N-(2-hydroxyethyl) salicylaldimine Schiff base as a ligand.

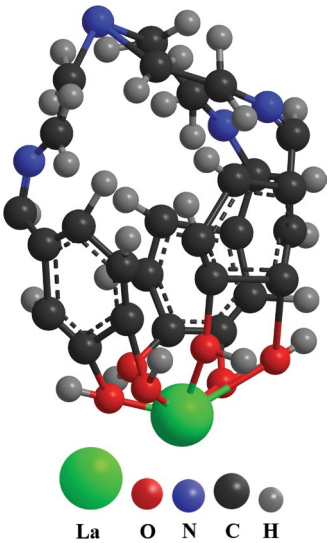

Fig. 18. Structure of lanthanum ions and tripod ligands.

the characteristics of the ligand but also has the commonality of the adsorbent, such as small size, large specific surface area and so on, and there are physical adsorption or chemical adsorption in the adsorption process. The process of La(III) being adsorbed is shown in Fig. 19.

4. Conclusion

In this study, by TEM, XRD and FT-IR characterization, we found that the magnetic tripod ligand was successfully synthesized. Single-factor experiments showed that the adsorption effect was the highest with a dosage of 1.6 g/L, time of 120 min, and a pH of 5. The selective adsorption experiments showed that the interfering ions had little effect on the adsorption of La(III). The interaction of various factors was considered. Moreover, in the RSM, the final model can explain the original experimental data well and can accurately predict the experimental results. The result predicted by the model is that the adsorption effect is optimal with a dosage of 0.8 g/L, time of 100 min, and pH of 5. Meanwhile, the removal rate is

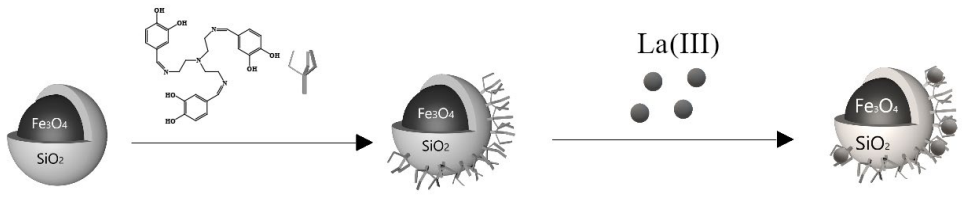

Fig. 19. Synthesis and adsorption schematic diagram of adsorbent.

99.42%. Moreover, the experimental results showed that the removal rate of lanthanum ion could reach 97.9%. Also, we verified the recyclability of the adsorbent. The results showed that the removal rate of La(III) decreased after five times of adsorption, but still reached 78%. In terms of the selective adsorption mechanism, we believe that it may be the result of the interaction of the adsorbent itself with the ligand.

Acknowledgements

This study has been received strong support from the National Natural Science Foundation of China (No. 51268018). The authors acknowledge the supporting provided by National Engineering Research Center for Domestic and Building Ceramics in Jingdezhen Ceramic Institute on analytical measurements.

References

[1] O. Tsydenova, M. Bengtsson, Chemical hazards associated with treatment of waste electrical and electronic equipment, Waste Manage., 31 (2011) 45–58.
[2] G. Chauhan, P.R. Jadhao, K.K. Pant, K.D.P. Nigam, Novel technologies and conventional processes for recovery of metals from waste electrical and electronic equipment: challenges & opportunities – a review, J. Environ. Chem. Eng., 6 (2018) 1288–1304.
[3] A. Lixandru, P. Venkatesan, C. Jonsson, I. Poenaru, B. Hall, Y. Yang, A. Walton, K. Guth, R. Gauss, O. Gutfleisch, Identification and recovery of rare-earth permanent magnets from waste electrical and electronic equipment, Waste Manage., 68 (2017) 482–489.
[4] G.J. Ruiz-Mercado, M.A. Gonzalez, R.L. Smith, D.E. Meyer, A conceptual chemical process for the recycling of Ce, Eu, and Y from LED flat panel displays, Resour. Conserv. Recyl., 126 (2017) 42–49.
[5] Y. Kim, H. Seo, Y. Roh, Metal recovery from the mobile phone waste by chemical and biological treatments, Minerals, 8 (2018) 1–10.
[6] S.R. Mueller, P.A. Wager, R. Widmer, I.D. Williams, A geological reconnaissance of electrical and electronic waste as a source for rare earth metals, Waste Manage., 45 (2015) 226–234.
[7] C. Agarwal, R.W. Cattrall, S.D. Kolev, Donnan dialysis based separation of gold(III) from electronic waste solutions using an anion exchange pore-filled membrane, J. Membr. Sci., 514 (2016) 210–216.
[8] A. Gurgul, W. Szczepaniak, M. Zablocka-Malicka, Incineration and pyrolysis vs. steam gasification of electronic waste, Sci. Total Environ., 624 (2018) 1119–1124.
[9] J. Bacher, A. Mrotzek, M. Wahlstrom, Mechanical pre-treatment of mobile phones and its effect on the printed circuit assemblies (PCAs), Waste Manage., 45 (2015) 235–245.
[10] L.A. Diaz, T.E. Lister, Economic evaluation of an electrochemical process for the recovery of metals from electronic waste, Waste Manage., 74 (2018) 384–392.
[11] S.M. Abdelbasir, C.T. El-Sheltawy, D.M. Abdo, Green processes for electronic waste recycling: a review, J. Sustain. Metall., 4 (2018) 295–311.
[12] S.M. Abdelbasir, S.S.M. Hassan, A.H. Kamel, R.S. El-Nasr, Status of electronic waste recycling techniques: a review, Environ. Sci. Pollut. Res., 25 (2018) 16533–16547.
[13] Y. Yao, N.F. Farac, G. Azimi, Supercritical fluid extraction of rare earth elements from nickel metal hydride battery, ACS Sustain. Chem. Eng., 6 (2017) 1417–1426.
[14] G. Zhongqun, Z. Kui, J. Jiefang, W. Guanshi, W. Xiaojun, Research progress on adsorption characteristics of rare earth ions by different adsorbents, J. Chinese Soc. Rare Earth, 36 (2018) 406–416.
[15] M.J. Page, K. Soldenhoff, M.D. Ogden, Comparative study of the application of chelating resins for rare earth recovery, Hydrometallurgy, 169 (2017) 275–281.
[16] C.M. Babu, K. Binnemans, J. Roosen, Ethylenediaminetriacetic acid-functionalized activated carbon for the adsorption of rare earths from aqueous solutions, Ind. Eng. Chem. Res., 57 (2018) 1487–1497.
[17] D.L. Ramasamy, E. Repo, V. Srivastava, M. Sillanpaa, Chemically immobilized and physically adsorbed PAN/acetylacetone modified mesoporous silica for the recovery of rare earth elements from the waste water-comparative and optimization study, Water Res., 114 (2017) 264–276.
[18] T. Ogata, H. Narita, M. Tanaka, Adsorption behavior of rare earth elements on silica gel modified with diglycol amic acid, Hydrometallurgy, 152 (2015) 178–182.
[19] W. Yang, Z. Xuefeng, Z. Baosheng, L. Zhong, L. Baoyi, Adsorption performance of mesoporous nanometer γ-Al_2O_3 to rare earth elements lanthanum and cerium, Chinese J. Environ. Eng., 6 (2012) 4519–4524.
[20] F. Qingqin, Preparation and adsorption properties of mesoporous nano-γ-Al_2O_3, Zhengzhou University, Zhengzhou, 2007 (In Chinese).
[21] Q. Guang-ri, Y. Lan-hao, P. Xu-li, H. Bin, J. Zu-cheng, P. Tian-you, Study on adsor ption behaviors of rare earth ions on nanometer Al_2O_3 powder by ICP-AES, J. Anal. Sci., 20 (2004) 337–340.
[22] M.M. Rahman, S.B. Khan, H.M. Marwani, A.M. Asiri, SnO_2–TiO_2 nanocomposites as new adsorbent for efficient removal of La(III) ions from aqueous solutions, J. Taiwan Inst. Chem. Eng., 45 (2014) 1964–1974.
[23] J. Roosen, K. Binnemans, Adsorption and chromatographic separation of rare earths with EDTA- and DTPA-functionalized chitosan biopolymers, J. Mater. Chem. A, 2 (2014) 1530–1540.
[24] M.M. Yusoff, N.R.N. Mostapa, M.S. Sarkar, T.K. Biswas, M.L. Rahman, S.E. Arshad, M.S. Sarjadi, A.D. Kulkarni, Synthesis of ion imprinted polymers for selective recognition and separation of rare earth metals, J. Rare Earth, 35 (2017) 177–186.
[25] D. Wu, Y. Sun, Q. Wang, Adsorption of lanthanum (III) from aqueous solution using 2-ethylhexyl phosphonic acid mono-2-ethylhexyl ester-grafted magnetic silica nanocomposites, J. Hazard. Mater., 260 (2013) 409–419.
[26] L. Molina, J. Gaete, I. Alfaro, V. Ide, F. Valenzuela, J. Parada, C. Basualto, Synthesis and characterization of magnetite nanoparticles functionalized with organophosphorus compounds and its application as an adsorbent for La (III), Nd (III) and Pr (III) ions from aqueous solutions, J. Mol. Liq., 275 (2019) 178–191.
[27] L. Jiang, W. Zhang, C. Luo, D. Cheng, J. Zhu, Adsorption toward trivalent rare earth element from aqueous solution by zeolitic imidazolate frameworks, Ind. Eng. Chem. Res., 55 (2016) 6365–6372.
[28] R. Zandipak, S. Sobhanardakani, Novel mesoporous Fe_3O_4/SiO_2/CTAB–SiO_2 as an effective adsorbent for the removal of amoxicillin and tetracycline from water, Clean Technol. Environ., 20 (2018) 871–885.
[29] D. Yan-jie, G. Ke, G. Xin-xing, Spectrophotometric determination of microamont of lanthanum with arsenazo, J. Chongqing Norm. U. (Nat. Sci. Edit.), 21 (2004) 43–45.
[30] S. Wen-xin, S. Ya-qin, L. Yong-lin, L. Xiang, Determination of total rare earth contents in Sm-Eu-Gd concentrate by EDTA volumetric method, J. Anal. Sci., 21 (2005) 343–344.
[31] M.A. Hafez, I.M. Kenawy, M.A. Ramadan, Titration of thorium and rare earths with ethylenediaminetetraacetic acid using Semimethylthymol Blue by visual end-point indication, Analyst, 119 (1994) 1103–1106.
[32] H. Shi, Y. Huang, C. Cheng, G. Ji, Y. Yang, H. Yuan, Preparation and characterization of chain-like and peanut-like Fe_3O_4@SiO_2 core-shell structure, J. Nanosci. Nanotechnol., 13 (2013) 6953–6960.
[33] W. Xie, C. Zhang, Production of medium-chain structured lipids using dual acidic ionic liquids supported on Fe_3O_4@SiO_2 composites as magnetically recyclable catalysts, LWT-Food Sci. Technol., 93 (2018) 71–78.

[34] G.H. Du, Z.L. Liu, X. Xia, Q. Chu, S.M. Zhang, Characterization and application of Fe_3O_4/SiO_2 nanocomposites, J. Sol-Gel Sci. Technol., 39 (2006) 285–291.
[35] M. Esmaeilpour, A.R. Sardarian, J. Javidi, Synthesis and characterization of Schiff base complex of Pd(II) supported on superparamagnetic $Fe_3O_4@SiO_2$ nanoparticles and its application as an efficient copper- and phosphine ligand-free recyclable catalyst for Sonogashira–Hagihara coupling reactions, J. Organomet. Chem., 749 (2014) 233–240.
[36] M. Esmaeilpour, A.R. Sardarian, J. Javidi, Schiff base complex of metal ions supported on superparamagnetic $Fe_3O_4@SiO_2$ nanoparticles: an efficient, selective and recyclable catalyst for synthesis of 1,1-diacetates from aldehydes under solvent-free conditions, Appl. Catal. A, 445–446 (2012) 359–367.
[37] J. Zucheng, C. Ruxiu, Z. Huashan, Rare Earth Element Analytical Chemistry, Science Press, Beijing, 2000 (In Chinese).
[38] N. Moradi, S. Salem, A. Salem, Optimizing adsorption of blue pigment from wastewater by nano-porous modified Na-bentonite using spectrophotometry based on response surface method, Spectrochim. Acta A, 193 (2018) 54–62.
[39] M. Zendehdel, B. Shoshtari-Yeganeh, H. Khanmohamadi, G. Cruciani, Removal of fluoride from aqueous solution by adsorption on NaP:HAp nanocomposite using response surface methodology, Process Saf. Environ., 109 (2017) 172–191.
[40] A.M. Zayed, A.Q. Selim, E.A. Mohamed, M.S.M. Abdel Wahed, M.K. Seliem, M. Sillanp, Adsorption characteristics of Na-A zeolites synthesized from Egyptian kaolinite for manganese in aqueous solutions: response surface modeling and optimization, Appl. Clay Sci., 140 (2017) 17–24.
[41] M. Mourabet, A. El Rhilassi, H. El Boujaady, M. Bennani-Ziatni, A. Taitai, Use of response surface methodology for optimization of fluoride adsorption in an aqueous solution by Brushite, Arab. J. Chem., 10 (2017) S3292–S3302.
[42] M. Dastkhoon, M. Ghaedi, A. Asfaram, A. Goudarzi, S.M. Mohammadi, S. Wang, Improved adsorption performance of nanostructured composite by ultrasonic wave: optimization through response surface methodology, isotherm and kinetic studies, Ultrason. Sonochem., 37 (2017) 94–105.
[43] B. Kakavandi, M. Jahangiri-rad, M. Rafiee, A.R. Esfahani, A.A. Babaei, Development of response surface methodology for optimization of phenol and p-chlorophenol adsorption on magnetic recoverable carbon, Microporous Mesoporous Mater., 231 (2016) 192–206.
[44] Y. Wu, Y. Jin, J. Cao, P. Yilihan, Y. Wen, J. Zhou, Optimizing adsorption of arsenic(III) by NH_2-MCM-41 using response surface methodology, J. Ind. Eng. Chem., 20 (2014) 2792–2800.
[45] S. Sun, J. Yang, Y. Li, K. Wang, X. Li, Optimizing adsorption of Pb(II) by modified litchi pericarp using the response surface methodology, Ecotoxicol. Environ. Saf., 108 (2014) 29–35.
[46] M. Arulkumar, P. Sathishkumar, T. Palvannan, Optimization of Orange G dye adsorption by activated carbon of Thespesia populnea pods using response surface methodology, J. Hazard. Mater., 186 (2011) 827–834.
[47] M. Xia, C. Ye, K. Pi, D. Liu, A.R. Gerson, Cr(III) removal from simulated solution using hydrous magnesium oxide coated fly ash: optimization by response surface methodology (RSM), Chinese J. Chem. Eng., 26 (2018) 1192–1199.
[48] S.S. Hussien, Biosorption of lanthanum from aqueous solution using Pleurotus ostreatus basidiocarps, Int. J. Biotechnol. Res., 2 (2014) 26–36.
[49] Z. Birungi, E. Chirwa, The kinetics of uptake and recovery of lanthanum using freshwater algae as biosorbents: comparative analysis, Bioresour. Technol., 160 (2014) 43–51.
[50] F. Zhao, E. Repo, Y. Meng, X. Wang, D. Yin, M. Sillanpaa, An EDTA-β-cyclodextrin material for the adsorption of rare earth elements and its application in preconcentration of rare earth elements in seawater, J. Colloid Interface Sci., 465 (2016) 215–224.
[51] S. Iftekhar, V. Srivastava, M. Sillanpää, Enrichment of lanthanides in aqueous system by cellulose based silica nanocomposite, Chem. Eng. J., 320 (2017) 151–159.
[52] X. Xu, X.-Y. Jiang, F.-P. Jiao, X.-Q. Chen, J.-G. Yu, Tunable assembly of porous three-dimensional graphene oxide-corn zein composites with strong mechanical properties for adsorption of rare earth elements, J. Taiwan Inst. Chem. Eng., 85 (2018) 106–114.
[53] A.A. Galhoum, M.G. Mafhouz, S.T. Abdel-Rehem, N.A. Gomaa, A.A. Atia, T. Vincent, E. Guibal, Cysteine-functionalized chitosan magnetic nano-based particles for the recovery of light and heavy rare earth metals: uptake kinetics and sorption isotherms, Nanomaterials (Basel), 5 (2015) 154–179.
[54] M. Butnariu, P. Negrea, L. Lupa, M. Ciopec, A. Negrea, M. Pentea, I. Sarac, I. Samfira, Remediation of rare earth element pollutants by sorption process using organic natural sorbents, Int. J. Environ. Res. Public Health, 12 (2015) 11278–11287.
[55] A. Tadjarodi, V. Jalalat, R. Zare-Dorabei, Adsorption of La(III) in aqueous systems by N-(2-hydroxyethyl) salicylaldimine-functionalized mesoporous silica, Mater. Res. Bull., 61 (2015) 113–119.
[56] F. Zhou, J. Feng, X. Xie, B. Wu, Q. Liu, X. Wu, R. Chi, Adsorption of lanthanum (III) and yttrium (III) on kaolinite: kinetics and adsorption isotherms, Physicochem. Probl. Miner. Process., 55 (2019) 928–939.
[57] F. Granados-Correa, J. Vilchis-Granados, M. Jiménez-Reyes, L.A. Quiroz-Granados, Adsorption behaviour of La(III) and Eu(III) ions from aqueous solutions by hydroxyapatite: kinetic, isotherm, and thermodynamic studies, J. Chem., 2013 (2013) 1–9.
[58] L. Mei, L. Zhaogang, W. Jinxiu, H. Yanhong, Rare Earth Elements and Their Analytical Chemistry, Chemical Industry Press, Beijing, 2009 (In Chinese).
[59] M. Liu, W.B. Yuan, Q. Zhang, L. Yan, R.D. Yang, Synthesis, characterization and DNA interaction studies of complexes of lanthanide nitrates with tris(2-[(3,4-dihydroxybenzylidene) imino]ethyl)amine, Spectrochim. Acta A, 70 (2008) 1114–1119.
[60] H. Guangyan, Introduction to rare earth chemistry, Science Press, Beijing, 2014 (In Chinese).